# 岩盤滲水對於室內試驗模擬與鐵立庫崩塌形狀及地形演變之影響

柯傑夫[1*], 卡艾瑋[2], 萊威廉[3], 林伯勳[4], 冀樹勇[5]

**摘　　要**　本研究採用現地觀察、航照分析及樹木年輪分析進行鐵立庫崩塌調查並同時應用影像分析方法進行室內崩塌模型實驗，以了解受局部孔隙水壓影響崩塌地之形狀及地形演變特性。經赴現地調查發現，鐵立庫崩塌地崩崖最上方的岩盤有持續滲水的現象。此外，經室內模型實驗顯示，局部高孔隙水壓對崩塌地形狀與形貌特性影響甚鉅，並隨著崩崖的發展，寬長比逐漸降低。此外，當坡腳開始滑動時，在上坡鄰近局部高孔隙水壓區發生圓弧形滑動。經航照分析發現，隨鐵立庫崩塌地演變，寬長比逐漸降低，此外進行樹木年輪分析結果發現，鐵立庫邊坡坡腳開始滑動時，在崩崖最上方鄰近所觀察到的岩盤滲水區發生圓弧形滑動。

關鍵字:岩盤滲水，崩塌形狀演變，崩塌地形演變，樹木年輪分析，影像分析

# Tieliku landslide, Northern Taiwan: Possible role of focused bedrock exfiltration tested using a laboratory analogue

Keck, J.[1*], Capart, H.[2], Wright, W.·[3], Lin, B.S.[4], Chi, S.Y[5].

**ABSTRACT** Field investigations, aerial photo analysis and tree ring analysis of the Tieliku landslide combined with results from a series of landslide tests using a laboratory-scale analogue and image analysis techniques were used to indentify topographic and geometric characteristics of landslides triggered by water exfiltrating from a localized area of bed rock. Water exfiltrating from weathered bedrock at the top of the final Tieliku landslide scarp was discovered during initial field investigations. The average width to slope distance ratio of the Tieliku landslide showed a decreasing trend as the scarp developed. Tree ring analysis of trees boarding the upper edge of the final scarp revealed that during the same year initial failure at the base of the slope occurred, the top of the hillslope, near the observed location of bedrock water, exhibited rotational failure. These failure characteristics match laboratory results for failures triggered by a point source of water.

***Keywords:*** bedrock exfiltration, landslide evolution, tree ring analysis, image analysis

---

〔1〕財團法人中興工程顧問社大地工程研究中心助理研究員（* 通訊作者 E-mail: keckje@sinotech.org.tw）
Assistant Researcher, Geotechnical Engineering Research Center, Sinotech Engineering Consultants
〔2〕國立臺灣大學土木工程學系 教授兼副主任
Professor, Dept. of Civil Engineering, National Taiwan University, Taipei, Taiwan
〔3〕中央研究院環境變遷研究中心 訪問學者
Visiting Research Fellow, Research Center for Environmental Changes, Academia Sinica, Taipei, Taiwan
〔4〕財團法人中興工程顧問社大地工程研究中心副研究員
Associate Researcher, Geotechnical Engineering Research Center, Sinotech Engineering Consultants
〔5〕中興工程顧問社大地工程研究中心 經理
Manager, Geotechnical Engineering Research Center, Sinotech Engineering Consultants

## Introduction

Soils saturated by heavy rains have increased pore water pressures and reduced shear strengths. The effect of rain is increased by topographic hollows which concentrate water and create localized zones of saturation(O'Loughlin, 1986). High hydraulic conductivity passages within the soil or bedrock can also lead to localized zones of high pore water pressures. Various natural phenomenon have been noted to be likely causes of the high hydraulic conductivity passages that lead to localized zones pore water pressure. Within the soil, channels burrowed by animals, or left behind by decaying roots provide one method(Pierson 1983). Cracks, created by quick wetting and drying cycles have been found to allow water to quickly penetrate from the soil surface to the underlying impermeable bedrock surface. Also, in sedimentary soils or soils defined by a layer of high hydraulic conductivity soil, the high hydraulic conductivity soil can also act as a passage for rapid flow of water and increased soil water pressures into lower hydraulic conductivity soils. (Jones, 1971) Bedrock cracks can channel ground water and allow it to flow relatively unrestricted down slope into an overlying topsoil. Earthquake faults, which cause bedrock cracking, can channel water(Kastning, 1977).

A number of studies have noted the existence and likely importance of soil and bedrock point sources of water on the occurrence of landslides. Pierson(1977) observed soil pipes at head of landslides during a landslide inventory. McDonnell(1980) found cracks near a landslide that allowed water to flow directly to bedrock. In Montgomery et al(2002), a landslide near Coos Bay Oregon was monitored with a field of peizometers and tesiometers during failure. After failure, examination of the failure scarp revealed that locations of bedrock cracks of flowing water corresponded to locations of the highest pre-failure peizometer reading. The authors concluded that the bedrock water likely caused the slope failure. Laboratory experiments investigating the effects of an isolated source(Peirson 1983) clearly illustrated how channels of high hydraulic conductivity can locally increase soil pore water pressures using an oil device.

Laboratory experiments using flumes have generally used rain and soil water inputs that simulate slope parallel flow. These flume studies have investigated the effects of density and effective cohesion(Eckersley,1990), porosity(Iverson, 2000), infiltration direction(Iverson, 1997), sample thickness(Wang and Sassa, 2001), grain size(Wang and Sassa, 2003) and variations in permeability(Lorenco, 2006) on failure mode, pore water pressure, and stresses within the experimental soil mass. Many of these studies used stress and shear stress transducers, load cells and tensiometers to quantify variations in experiment behavior. Wang and Sassa(2001) quantified the movement of flow slides by tracking the movement of a styrene ball embedded in the flow slides by measuring movements of a wire attached to the ball using a displacement transducer. Millimeter precision topographic data sets of the geomorphic processes associated with hillslope water exfiltration were used by Ni and Capart(2005) and Huang, Huang and Capart(2010).

This report investigates the effect of infiltration direction on landslide geometric and topographic evolution. Both rain and ground water are tested, however, ground water is in the form of an isolated point source. Effects are monitored on a wall-less model hillslope rather than a flume, allowing geometric and topographic evolution and failure mode of the unconfined landslide to be observed. Sand conditions and point source flow were carefully controlled and monitored to ensure consistency between experiments. Tests were performed on two different types of topographic hollows, allowing direct observation of topographic effects as well. Observations were quantified using detailed DTMs of various stages of failure obtained using image analysis techniques from Ni and Capart(2005). In addition to laboratory experiments, results were compared to landslide investigation results of the Tieliku Landslide.

A point source of water emanating from fractured bedrock at the top of the landslide scarp was located in the field. The failure process and dimensions of the landslide were quantified using aerial photographs, topographic maps and onsite survey measurements. A second survey of the landslide was made to look for upslope movement of the hill slope before actual formation of the failure scarp. This stage of the investigation was completed by performing tree ring analysis on trees boarding the upper edge of the scarp.

## Study Area

The Tieliku landslide retrogressively failed over a period of at least 11 years along the center of a north facing triangular faceted spur in the northern Xueshan mountains. The northeast southwest running Xueshan mountain range is formed as a result of techtonic uplift rather than volcanic activity, and is better described as a high elevation ridge system rather than a series of solitary peaks. Nearly continuous positive slope gradients can be traced from the Tieliku landslide to the highest mountains in the Xueshan mountain range which reach altitudes of more than 3700 meters. Slate and meta-sandstone make up the majority of the mountain range which is also crisscrossed with tectonic faults.(徐美玲, 2008) The crown of the Tieliku landslide has an elevation of 1275 meters and lies at the apex the spur. The landslide scarp has an average slope of 31.4 degrees, slope distance of 600 meters, average width of over 100 meters and estimated depth of 10 meters. Two fault lines lie within several kilometers of the Tieliku slope failure, one north of Tieliku, running east-west and a second fault, located south of Tieliku runs northeast-southwest. The location of fault line south of Tieliku is approximated and could be closer or farther from Tieliku. (Figure 1)

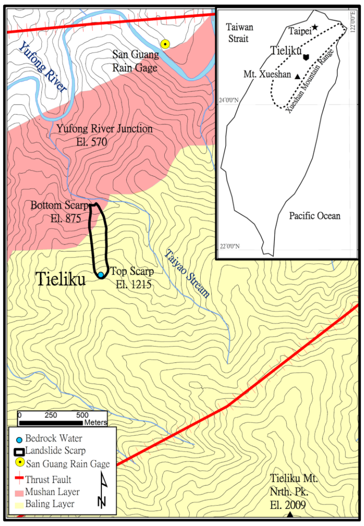


**Fig.1 Location, geologic and topograhic features of Teiliku landslide**

The Baling layer, a layer primarily composed of Argillite defines the local geologic setting near Tieliku. In Taiwan, Argillite has a high landsliding rate relative to other geologic bedrock types (Hua,2005). Soils boardering the Tieliku landslide are shallow and rocky. Like many deep landslides, the Tieliku landslide occurred in heavily fractured and weathered bedrock and not soil. Material left behind in the scarp is a boulder laden shale and slate gravel. Exposed intact bedrock along lower edges of the scarp are heavily fractured and highly permeable. Based on a 1985 obliquely lit aerial photograph and a 1994, 10 meter contour map, the pre-failure surface topography of Tieliku, though not an obvious topographic hollow, was slightly converging along the whole slope. The area available to collect rain fall and drain to Tieliku as slope parallel subsurface water flow, only includes a small 0.22 km2 drainage area defined by the top of the spur and upper ridge. Due to the structure of the Xueshan mountain range, preferential flow within fractured bedrock, soil pipes, or some other locally high hydraulic conductivity conduit , such as those near fault lines, could have a much larger drainage area.

## Landslide History

A visible landslide scarp did not appear in the aerial photo record until after the 1997 Typhoon Herb. The scarp initially began at the base of the spur, possibly at the cut-bank of the road that also first shows up in 1997. During the following 5 years, the scarp developed small heads of up- slope growth , but by 2005, primary scarp expansion was lateral as the scarp became more round in appearance. In 2006, the scarp suddenly exploded up the spur, reaching the apex of the spur. However, a large, forested block of unstable material was left hanging in the scarp. By 2008, the large forested block was completely evacuated from scarp. (Figure 2)

The outer edge of the landslide scarp measured from all available orthocorrect aerial photograph years(not all shown in Figure 2) is plotted in a single scarp progression plot and presented with cumulative rainfull data, collected from a Taiwan Water Resource Agency tipping bucket rain gage near the Tieliku landslide(Location shown in Figure 1) for the Typhoon storm events that occurred during failure activity of Tieliku landlide. The Typhoon name is plotted next to events which had hourly rain intensity and accumulated rain  that met the Soil and Water Conservation standard for "Extreme Heavy Rain".[CWB Website]. In the Tseng Wen watershed of southern Taiwan, "Heavy Rain" events have been found to account for only 49% of the total precipitation amount but 68% of the total annual sediment load.

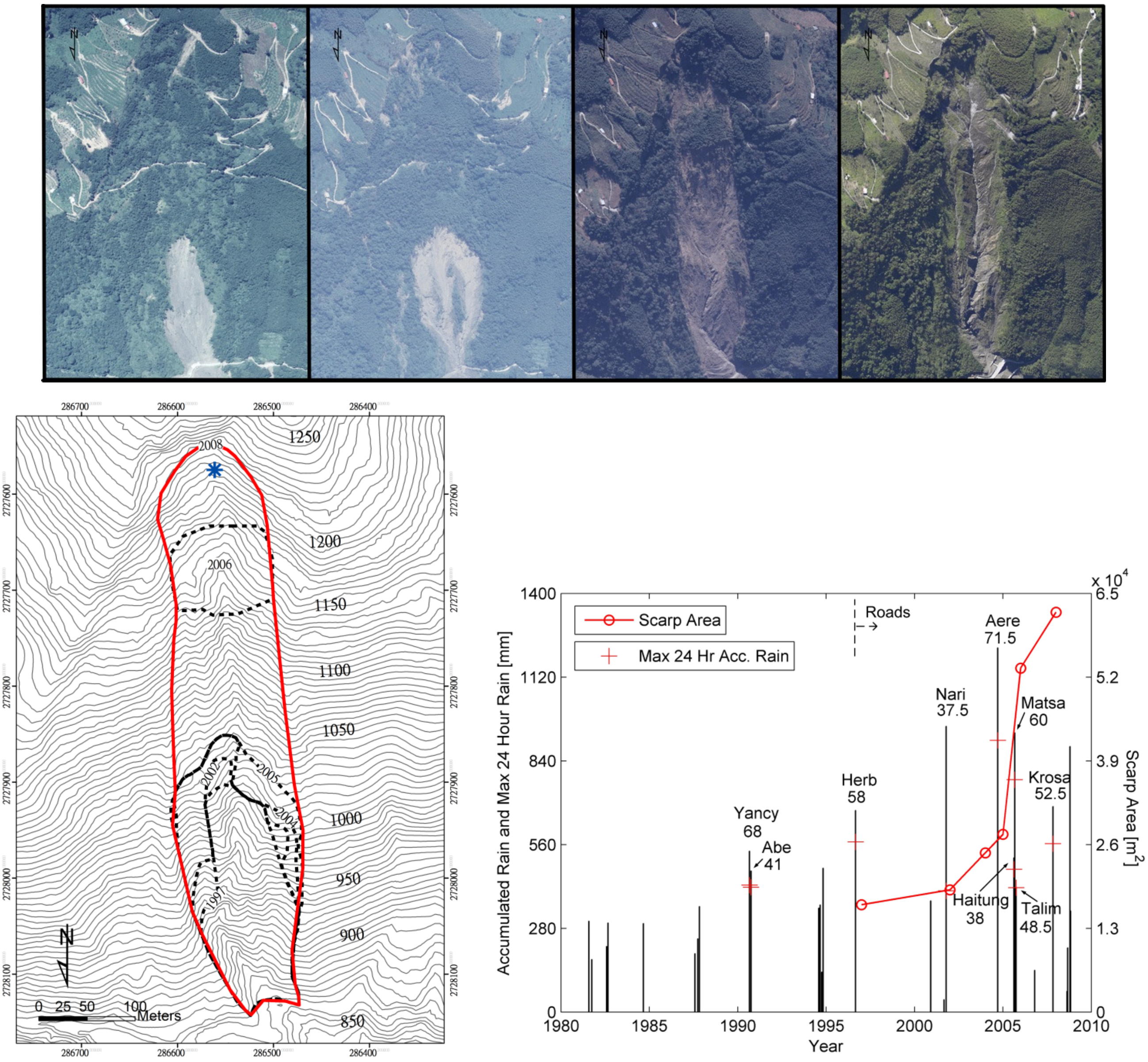


**Fig. 2 Top: Scarp history of Tieliku for the year 1997,2005,2006 and 2008 Left: Scarp progression plot for Tieliku. Note 2006 scarp is the same as 2008 except for the block left hanging at the top of the scarp. Contour interval is 5 meters. Star at top of scarp is GPS location of point source located in the field. Right: Total accumulated rain for all Typhoon events, maximum 24 hour and hourly rainfall rain(number below event name) for Typhoon events that meet "Extreme Heavy Rain" standards. Total Area of the landslide scarp relative to time is also plotted.**

## Analogue Hillslope Model

### *Overview of experimental procedure*

Retrogressive slope failure was initiated on a on a 130 cm long, 90cm wide laboratory analogue hillslope model (Figure 1). A total of 6 experiments were performed, contrasting 3 soil water situations on two different types of convergent bedrock topography or topographic hollows. Water was either input as downward vertical infiltration through the surface of the hillslope via a sprinkler system or as a focused point source of bedrock exfiltration, emanating from a 1cm diameter pipe placed parallel along the model bedrock surface near the top of the model(Figure 1, X-sex A-A', Figure 2, Top). Simultaneously using both water input methods was the third water input method. The model hillslope was wide enough that all failures developed within the slope, without boundary effects of walls or edges.

Before implementation of the 6 experiments used for analysis in this report, a series of tests were performed to identify basic model parameters such as grain size, sand depth, bedrock topography, sprinkling rates, point source flow and slope that would permit the model to fail in a manner similar to full scale landslides. Image measurement systems, which were used to obtain high precision, sub-millimeter accuracy digital topography models(DTMs) of experimental results were checked and fine tuned during preliminary tests which helped guarantee accurate and consistent measurement during the final 6 experiments. Model parameter values for the 6 experiments are listed in Table 1 and the series of tests are detailed in Keck and Capart, 2010. Measurements pertaining to the topography and geometry of the landslide were obtained using image analysis methods.

### *Image Measurement System*

Two cameras were used to record and perform measurements. An overhead high resolution single lens reflex camera, titled the ‘overhead camera’ and a lower resolution video camera titled the ‘topography camera’ The topography camera, which recorded 15 images per second was used to generate high detail, millimeter accuracy topography maps of the hillslope after failure using an image 3D measurement method described in Ni and Capart(2005) and Huang, Huang and Capart(2010). The overhead camera, recorded an image every second during failure and was used to record aerial photo like images of the model slope failure and provided results similar full size landslides. A clock, started at the beginning of each experiment and placed within the view range of the overhead camera allowed all overhead images to be time referenced. allowing later time identification of surface changes. This camera was also used to measure point source flow using the same 3D interpolation method used to measure topogrpahy. Camera locations are shown in **Figure 1.**

### *Weathered Bedrock(sand) and Solid Unweathered Bedrock(hillslope board)*

A coarse sand of median diameter D50 = 0.6mm diameter sand was used as the weathered bedrock layer. A wavy shaped roofing board with the same sand glued onto the surface served as the solid, unweathered bedrock surface. The sand had a capillary rise of approximately 3 cm and hydraulic conductivity of 0.33cm/s as determined through direct observation using florescent dye water under black light illumination and 9 permeameter tests in Ni and Capart(2005). The sand had an estimated friction angle of 0.31 as determined by the angle in which sliding occurred between two acrylic plates, both glued with the sand. The sand was placed in 5 liter lifts onto the horizontally positioned hillslope board. The sand was raked into place to an approximate depth of 6 cm but depth did systematically vary according to bedrock topography as indicated in sand placement diagrams shown in the left and right bottom figures of Figure 2. This soil depth distribution was roughly based on typical soil depth and topography relationships. Depths were high in the center of the hollow and thinner along the walls of the hollow.

The sand was not compacted except for the little that occurred when raking the soil into place and smoothing the surface. To make hydraulic and strength qualities of the placed soil as homogeneous as possible, equal amounts of raking and smoothing were applied over the whole surface of each experiment and a systematic method for controlling the water content of the sand(Keck and Capart, 2010) was used. Soil porosity and water content was recorded for the sand by collecting one to two samples from the upper corners of the model hillslope using methods similar to those described in Dane,2002) and ranged from 0.54 to 0.58. Water contents of the 6 experiments ranged from 0.09 to 0.11. Soil contraction resulting from initial wetting and downward creep of the sand during failure at the foot of the slope was observed and the average settlement along centerline of the slope was calculated using DTM measurements for initial conditions and conditions just after failure at the foot of the slope for each experiment(Figure 1, cross section A-A'). Soil contraction caused 0.4 mm to 1.2 mm of settlement, resulting in a decrease in porosity of 0.01 to 0.02(Table 1)

**Table 1 Experiment Parameters**

| Experiment Title | PST1 | RainT1 | RainPST1 | PST2 | RainT2 | RainPST2 |
|---|---|---|---|---|---|---|
| Water Input Method | Point Source | Rain | Rain + Point Source | Point Source | Rain | Rain + Point Source |
| Bedrock Topography | Topo 1 | Topo 1 | Topo 1 | Topo 2 | Topo 2 | Topo 2 |
| Number of Storm Events | 6 | 6 | 5 | 7 | 6 | 4 |
| Average Water Rainfall Rate(L/min) | NA | 5.10 | 5.10 | NA | 5.10 | 5.10 |
| Average Point Source Flow (L/min) | 2.35 | NA | 2.55 * | 2.37 | NA | 2.11 |
| Average Storm Length (min) | 2.3 | 4.2 | 1.5 | 1.8 | 4.6 | 1.6 |
| Sum of Storm Durations (min) | 14 | 25.1 | 7.6 | 12.5 | 27.8 | 6.3 |
| Total Water Input (L) | 32.9 | 128.0 | 58.1 | 29.6 | 141.8 | 45.4 |
| Pre-Failure Sand Properties | | | | | | |
| Average sand depth along centerline(perpendicular to slope) (cm) | 6.33 | 6.79 | 6.45 | 6.83 | 6.52 | 6.81 |
| Water content (%) | 0.10 | 0.10 | 0.08 | 0.10 | 0.08 | 0.08 |
| Bulk density (g/cm^3) | 1.13 | 1.15 | 1.16 | 1.22 | 1.16 | 1.16 |
| Porosity | 0.58 | 0.57 | 0.56 | 0.54 | 0.56 | 0.56 |
| Void ratio | 1.35 | 1.30 | 1.29 | 1.18 | 1.29 | 1.29 |
| After failure at base of slope and contraction of upper-slope | | | | | | |
| Settlement(perpendicular to slope) (cm) | 0.07 | 0.04 | 0.08 | 0.08 | 0.05 | 0.12 |
| Estimated porostiy | 0.56 | 0.56 | 0.55 | 0.53 | 0.55 | 0.54 |

*Note: RainPST1 P.S. flow measured at flume. All other experiments measured from observation pipe.

***Bedrock Topograpy***

Two types of converging bedrock topographies were selected to model the slightly converging surface topography found at Tieliku. For note keeping, the two topographies were titled “Topo 1” and “Topo 2” Descriptions of those topographies are detailed in the bottom of Figure 2. Contours for the bedrock and shading representative of soil depth are provided. All topographic values are referenced to the coordinate system axis located at the lower back left corner of the stainless steel frame (Figure 3).

Here the experimental setup and micro-topography of the model solid bedrock surface should be further explained. The wavy shaped fiberglass roofing board had a two centimeter trough to crest height and was attached by over 150 30 cm long screws to a tilting frame(visbile in figure 2, Top). Due to the flexibility of the fiberglass board, the topography of the board could to be adjusted when unsecured and then made rigid when secured by the screws, allowing relatively quick modification of bedrock topography from Topo1 to Topo2. Using the wave shaped fiber glass board forced model hillslope failure to occur in the sand and not along the base of the board, as shown in X-sec. 2 of Figure 3. Topographic plots of the two bedrock topographies are shown in the Figure 4 left and right figures.

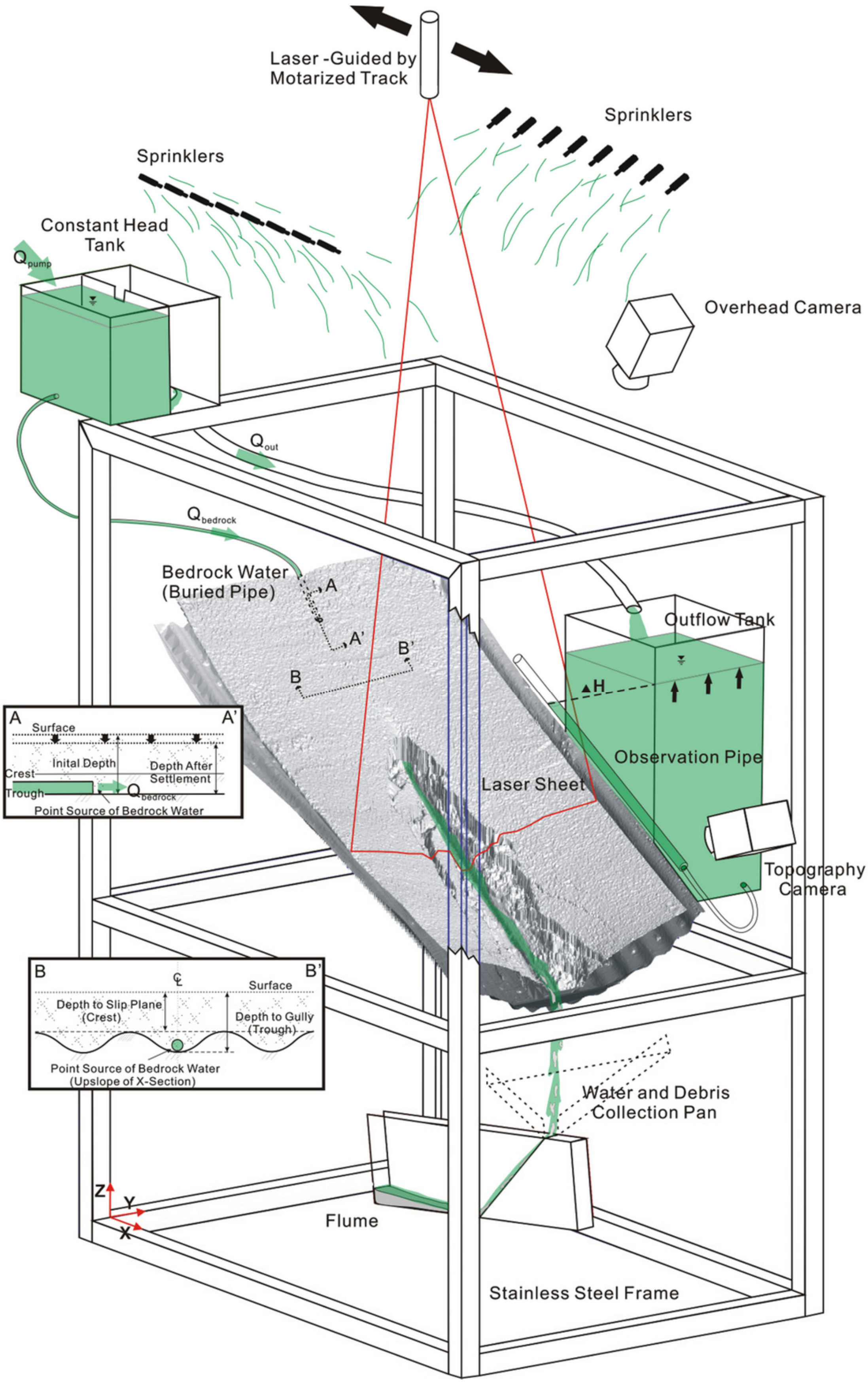


**Fig.3 Model hillslope and measurement system. X-Sec A-A' is a side view of the point source. X-Sec B-B' is shows the how depth is measured and the location of the point source and landslide slip plane.**

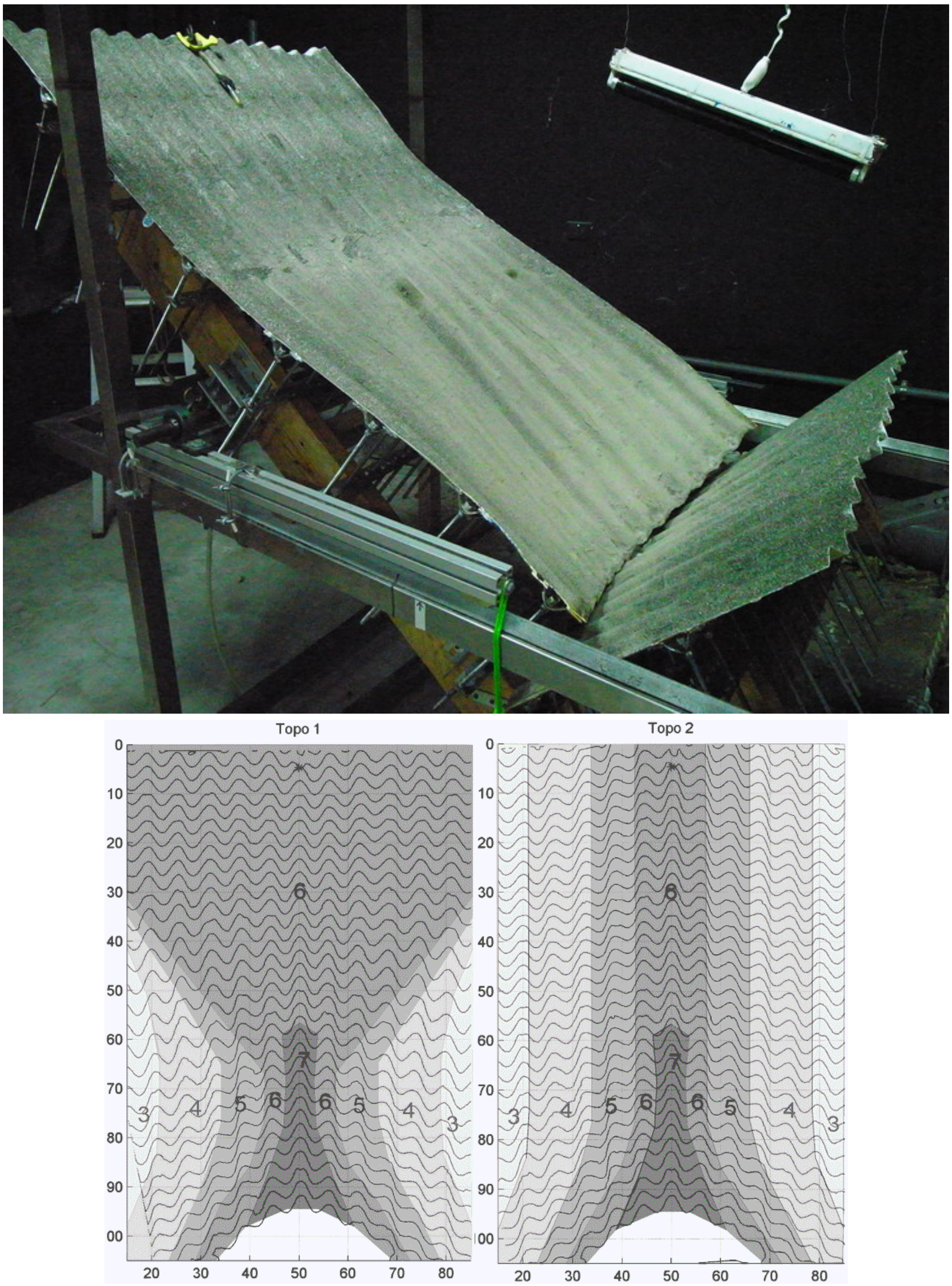


**Fig.4 Top: Model hillslope bedrock board. Upper figure shows board in Topo1 configuration and location of point source. Note, the outlet has not been set to the 24 cm width used for the experiemnts. The screws below the board, when fixed allow the board to be rigid. The screws attach to a tilting frame. Lower Left: Topo1 2 cm contours and approximate sand depth(numbers on board). Lower Right: Topo2 with 2 cm contours and approximate sand depth.**

### *Water Input and Flow Measurements*

A total of 16 sprinkler heads were used to simulate rain, 8 on each side of the slope(Figure 3), spread out along the length of the slope to ensure roughly even water distribution over the whole slope surface. Rain from the sprinklers was more a heavy mist, and easily influenced by otherwise unnoticeable air currents in the Laboratory. Resultantly, the entire experiment was wrapped in plastic sheeting to ensure a constant rainfall distribution on the slope. A constant water head tank supplied flow to the pipe that served as the point source, which was buried at the top of the slope, parallel to the slope board. A double valve system was used to control flow to the pipe, which helped ensure flow for all experiments was roughly constant. Sprinkler and point source location and direction of flow from the point source are detailed in Figure 3 and Cross section A-A' of Figure 3. Roughly constant flow was confirmed by measuring changes in the water depth of the adjacent outflow tank, which was performed using the overhead camera. Before and during each experiment, flow from the pump($Q_{pump}$) was measured when the point source was closed. The cross sectional area of the tank in the horizontal plane ($A_{tank}$ )was also measured which allowed point source flow($Q_{ps}$) to be monitored using the overhead camera and the following relationship:

$$Q_{ps} = Q_{pump} - \frac{dH}{dt} A_{tank} \tag{1}$$

The hyetograph applied to the model hillslope was designed to roughly mimic the 10 year history of typhoons that most likely influenced Tieliku. Based on the number of 'extreme heavy rain' events and aerial photo records, 5 to 6 storms were assumed to have controlled the failure of Tieliku. Time between major typhoon events at Tieliku varied from 2 weeks to several years. The importance of short term rain fall intensity relative to accumulated rain as a trigger for landsliding has been observed in Hong Kong and Oregon(Cornforth, 2005) It was therefore assumed that the rain intensity was the primary influential factor of the storm and that time between typhoon events was not a significant influence upon the landslide shape and failure process. During the experiment, time between storm events varied between 10 and 20 minutes. The assumption that time between storm events could vary was also made out of the practicality of needing time to measure the hillslope during the failure process; time between storm events was used to obtain topography measurements.

Although slope, topography, outlet conditions and rates of water input were controlled and sand was prepared and placed in the same way for each experiment, landslide behavior was still variable enough that it was difficult to determine exactly what length of storm would allow the landslide to fully evolve in 6 storm events. An approximate storm length of 2 minutes, as determined from the series of preliminary tests was used, however landslide storm duration ended up ranging from 1 to 2 minutes for point source landslides and 2 to 4 minutes for rain landslides.

***Sediment production, Surface Deformation and Scarp Expansion Plots***

Once topographic data sets were obtained for all stages of failure, sediment production associated with each storm was determined. Topographic data sets were constructed using the same n by n grid size. Subtraction of one data set from the other, and then multiplication by grid area gave the failure volume(pore and solid space) for each storm(Equation 2). Sediment production was quantified by multiplying the failure volume by the solid fraction of the soil(Equation 3). Surface changes on the slope outside of the landslide scarp were quantified by subtracting DTM data from the initial conditions DTM data using equation 4. DTM data sets were viewed in the horizontal plane and the edge of the scarp traced to produce the Scarp Expansion plots. For equations (12) and (13) $\Delta V$ is the change in slope volume, i is the column number, or location along the X axis of the grid, j is the row number or location along the Y axis of the grid and $t_k, t_{k-1}$ and $t_1$ corrispond to the dtm data set number, with t1 being initial conditions. $\delta a$ is the grid size used for the dtm, which in the case of the dtm data sets used in this study was 1mm.

$$\Delta V = \sum_i \sum_j \left( z_{dtm}(x_i, y_j, t_{k-1}) \quad z_{dtm}(x_i, y_j, t_k) \right) \delta a \tag{2}$$

$$S = \Delta V_{*(1-n)} \tag{3}$$

$$\Delta z_{dtm}(x_i, y_j, t_k) = \left( z_{dtm}(x_i, y_j, t_1) - z_{dtm}(x_i, y_j, t_k) \right) \tag{4}$$

## Model and Field Results

### *Scarp Progression*

**Scarp** progression plots(outlines of the scarp after each storm event) for each experiment are plotted on top of initial surface topography for each experiment in Figure 5. Scarp progression is visually quantified by plotting the average width to slope distance ratio (W/SD) relative to slope position(l/L). Slope distance of the scarp is the distance between the foot and the upper edge of the scarp. Slope position is described as the horizontal length of the scarp(l) divided by the horizontal distance between the foot of the scarp and top of the hillslope (L), which is defined by a topographic divide. Average width is the scarp area, divided by scarp length, both measured from the DTM data sets in the horizontal plane.

Scarp progression for the point source only experiments (PST1 and PST2) was dominated by narrow, upslope scarp growth, which narrowed as the landslide neared the top of the slope as demonstrated by the decreasing W/SD ratio relative to slope position in Figure 6. In both cases, scarp expansion ended with a sudden piece or block like failure from the top of the slope, near the point source. Block like failure in experiment PST1 ran down the existing scarp, only slightly increasing the size of the scarp as it contacted the scarp edge. Final block like failure in experiment PST2 was initially about the same size as that of PST1. However, upon contact with the adjacent scarp walls, the failure piece caused a domino effect, resulting in mass failure and sediment production along the upper edge of the failure scarp.

Initial scarp expansion for RainT1 and RainT2 was similar to that observed in the point source experiments. However, during later storms, lateral expansion nearly equaled upslope scarp growth. This is demonstrated by the constant W/SD ratios with position on the slope, in Figure 6(left). During the final, purposely long rainfall amount, both RainT1 and RainT2 are dominated by lateral growth, causing an increase in the W/SD ratio without very little change in position on the slope. Sudden block like failure, like that observed in the point source experiments, is never observed in the rain experiments.

***Landslide volume(Sediment Production):***

Landslide volume is plotted relative to slope position in Figure 6(right). Landslide volume for the Tieliku landslide is also plotted using a separate axis and the assumption that landslide depth was constant at 10 meters for the entire landslide process. All landslides (including Tieliku) share a common feature: initial landslide volume at the base of the slope is large relative to subsequent landslide volumes that occur further up the slope. For the rain experiments, if the final purposely long rain events are ignored, the initial landslide volume accounts for the majority of the overall sediment produced by the landslide. After initial failure, Landslide volumes for the PS experiments are small, like the rain experiments, but once the landslide scarp nears the point source of bedrock water, landslide volume is suddenly large and a mass flux of sediment is flushed down the slope.

***Surface Deformation Plots***

Two trends are observed in the surface erosion plots: the existence and non-existence of hillslope movement above the landslide scarp. All experiments show movement adjacent to the landslide scarp. However, Rain experiments show no evidence of movement upslope of the scarp while the PS experiments do show movement far upslope of the scarp at the location of the point source of bedrock water.

Upslope deformation is pronounced in the Topo2 experiments and experiments that have both rain and bedrock water inputs. Deformation includes settlement and rotational caused bulging. Deformation on the hillslope seems to give an impression of the flow paths of the water emanating from the point source. The top row of Figure 1 shows PST1. A circular pattern of settlement occurred just below the point source. The top of the circle is intersects the tip of the point source and base of the circle is located where the topography converges. A very clear rotational feature is observed in experiment RainPST2 just below the point source. Overhead camera images of the final block like failure of RainPST2 is shown in Figure 6.

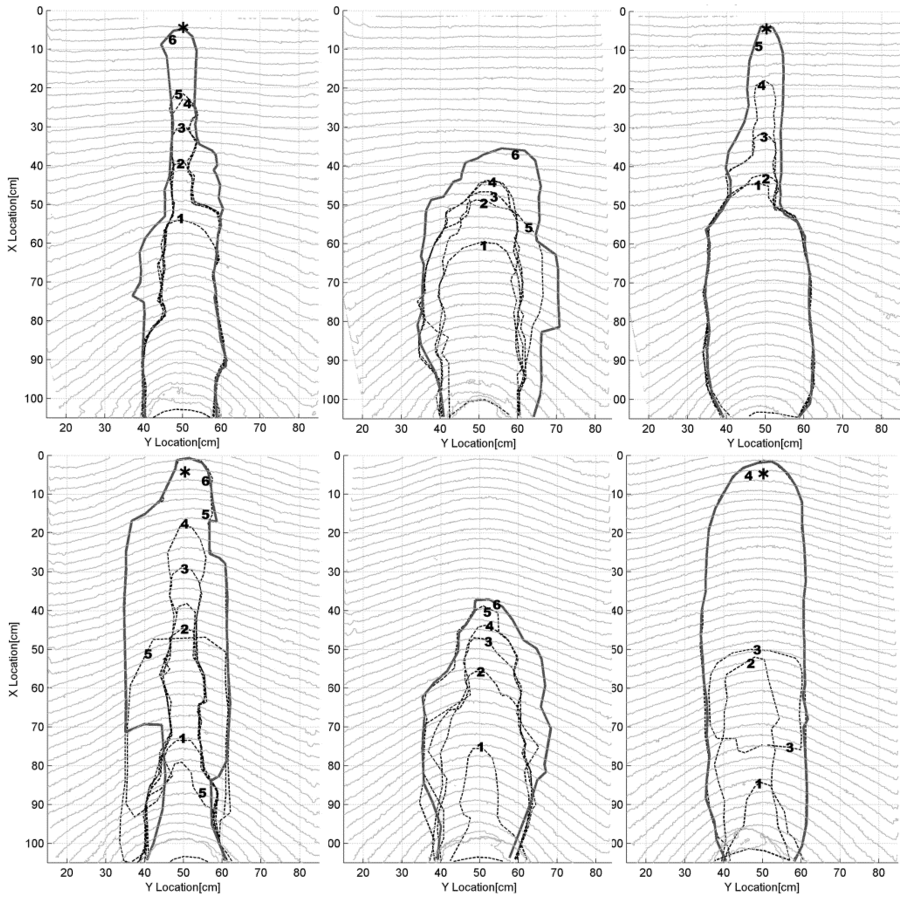


**Fig.5 Scarp progression plots for all six experiments. From the top left corner, clockwise, the experiments are PST1, RainT1, RainPST1, RainPST2, RainT2 and PST2.**

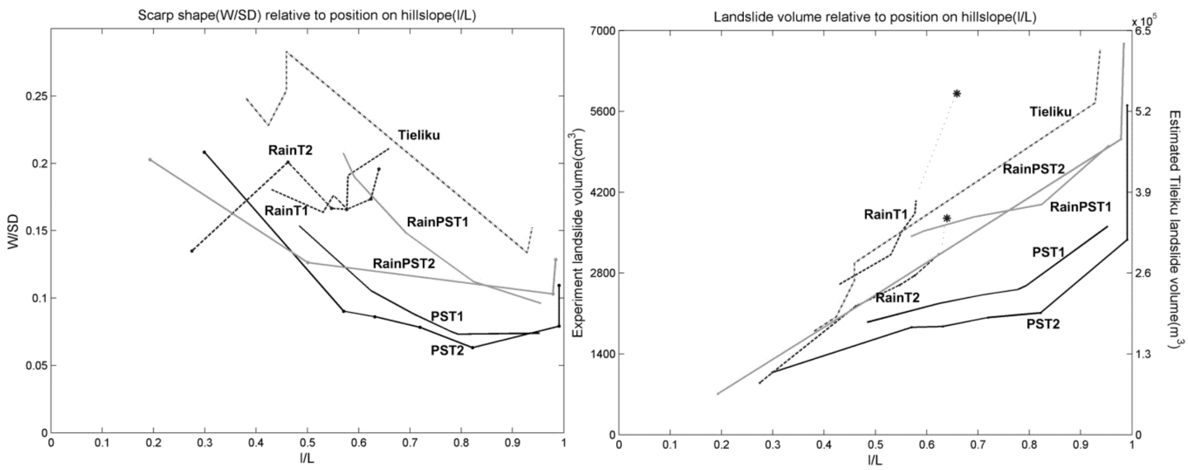


**Fig. 6 (Right) W/SD ratio relative to slope position(l/L). (Left) Accumulated landslide volume relative to slope position. Data from the Tieliku landslide is included in both plots.**

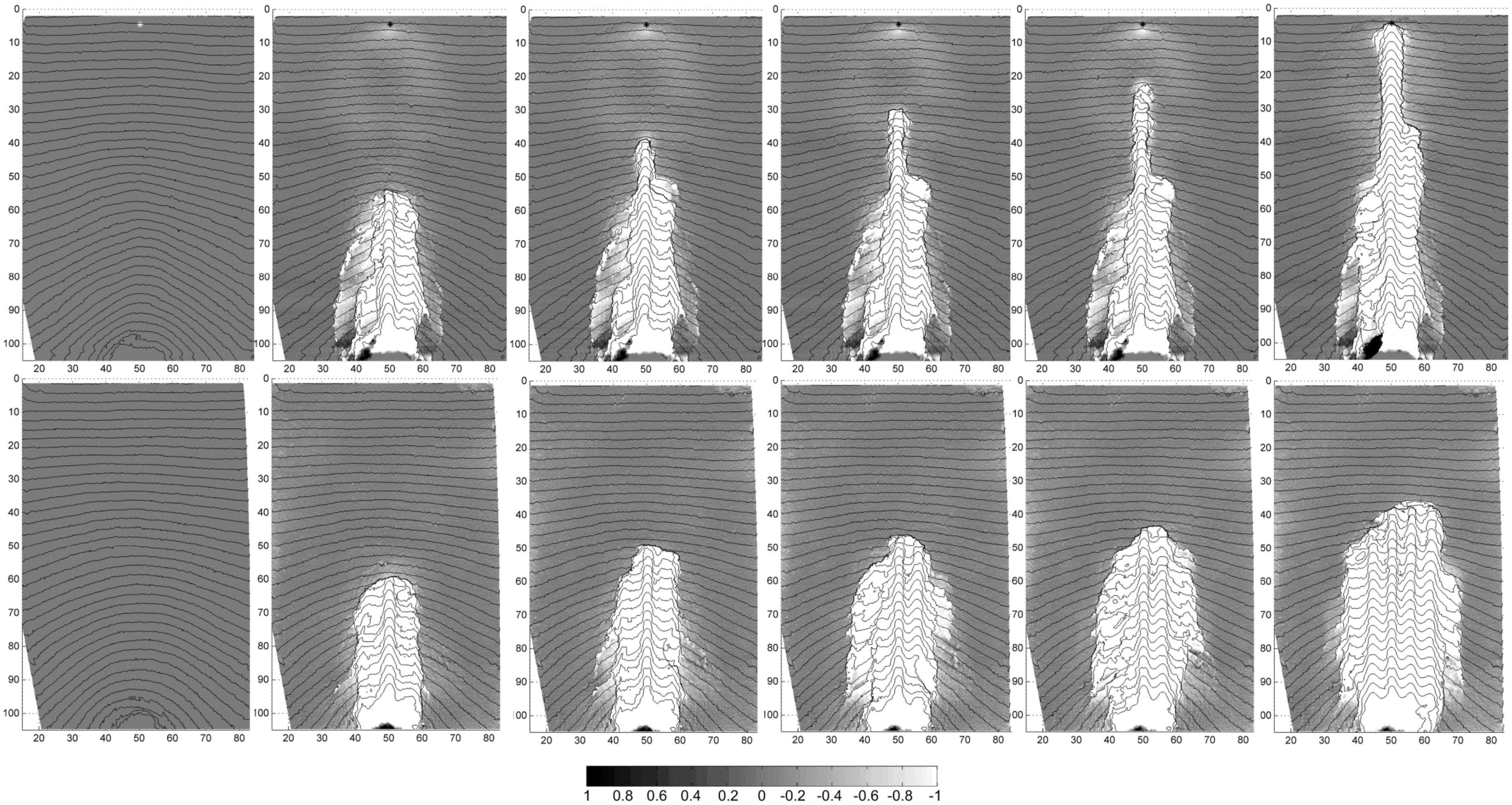


**Fig. 7: PST1(top) and RainT1(bottom) deformation plots. All units are in cm.**

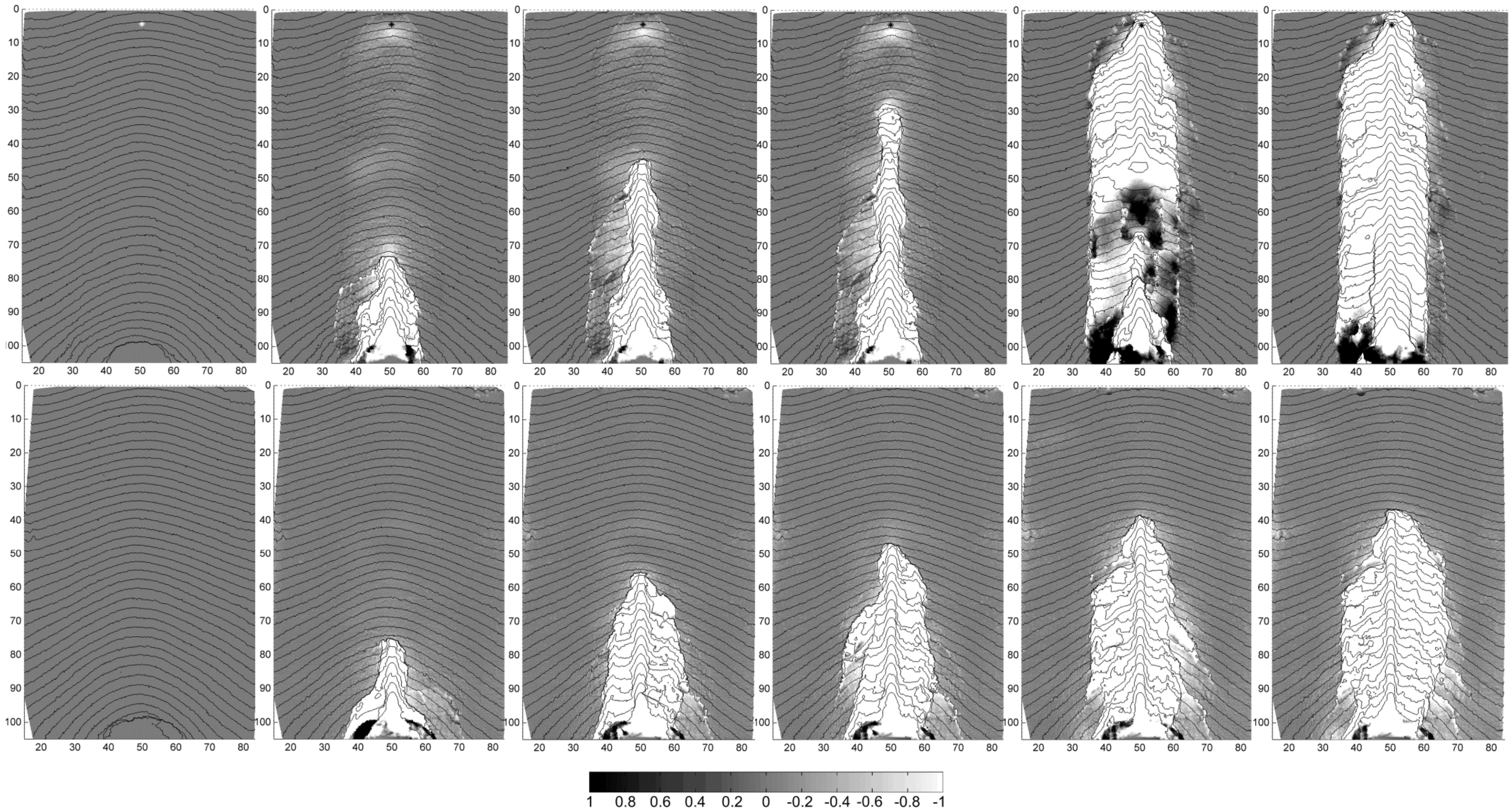

**Fig.8: PST2(top) and RainT2(bottom) deformation plots. All units are in cm**

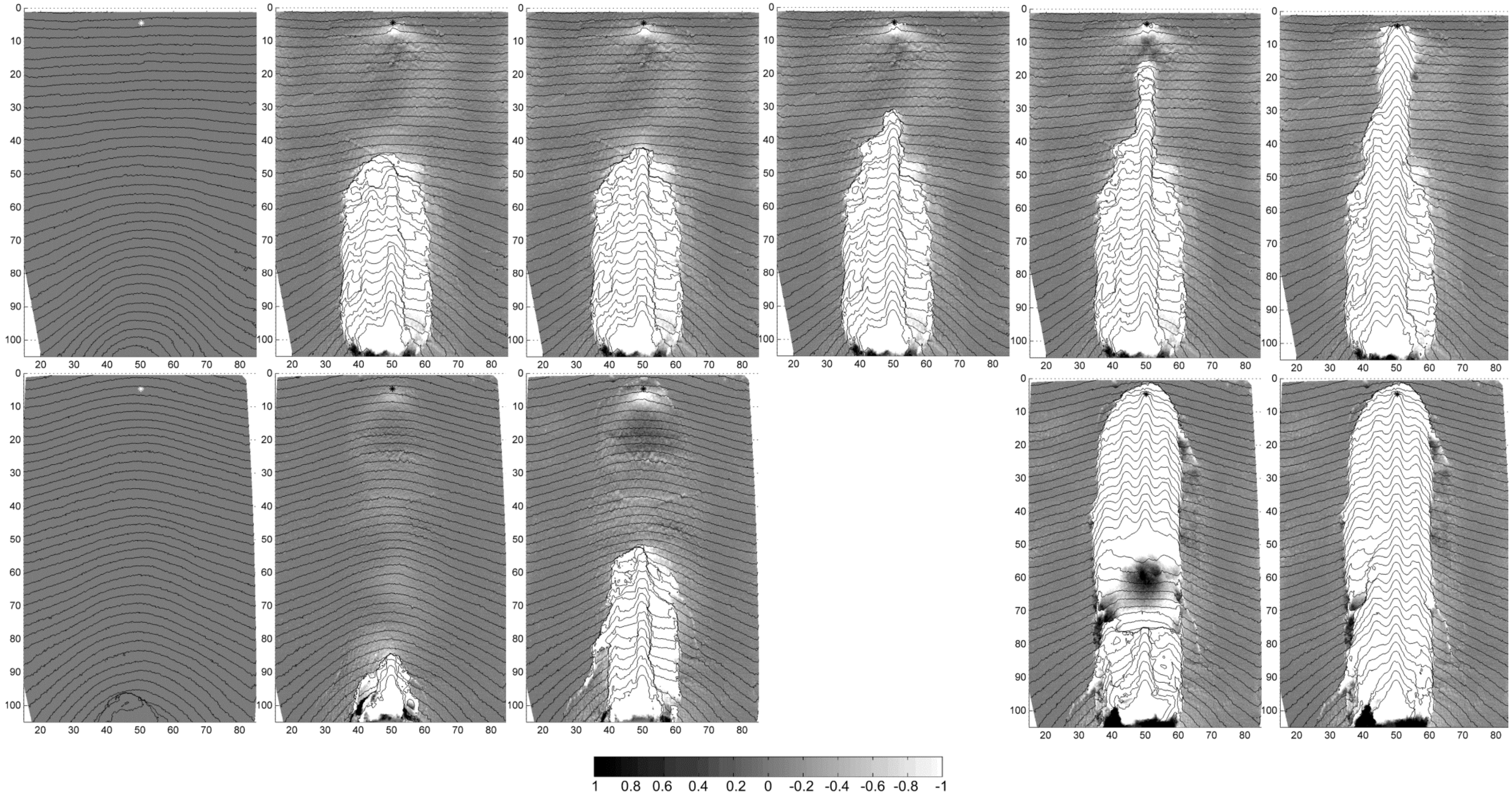

**Fig. 9: RainPST2(top) and RainPST2(bottom) deformation plots. All units are in cm.**

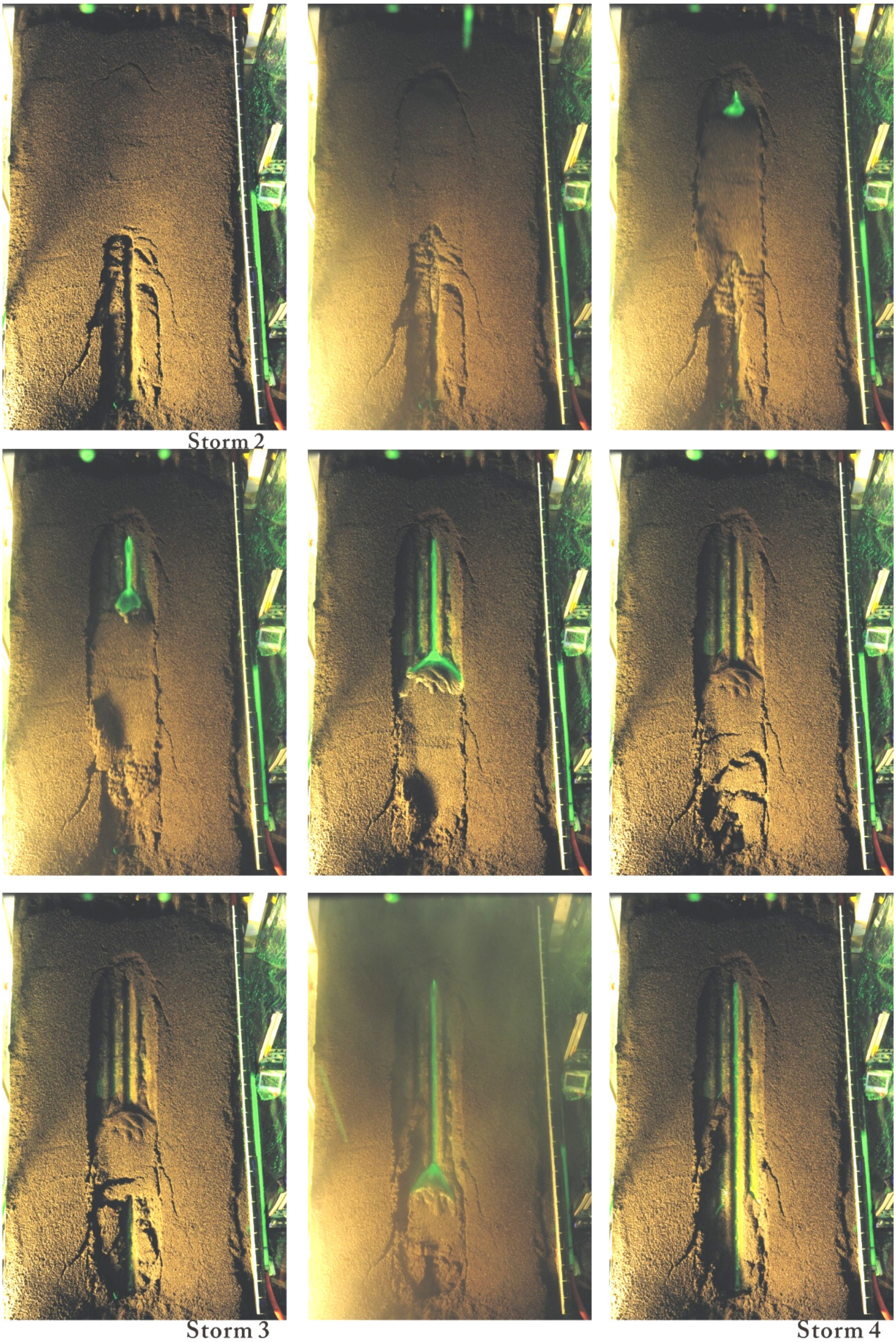


**Fig. 10: Overhead camera shots of the failure process between storm events 2 and 4**

## Surface displacement above the Tieliku landslide based on tree ring record

A secondary survey trip to the Tieliku landslide was made to look for signs of upslope movement, similar to that observed in the PS experiments. To obtain time referenced data of past hillslope movement, a tree ring survey was performed. Based on experiment results, it was decided to sample all available trees directly boarding the suspected point source

Many types of trees grow annual tree rings. Variations in the width of the ring can allow inferences regarding environmental conditions with which the tree was growing. Tree rings are generally symmetric about the center of the tree. If the tree experiences a force that causes bending at the base of the tree, another type of wood grows, called reaction wood. Reaction wood is what allows disturbances such as landslides and creep to be dated.[Schroder, 1978]

Tree lean depends on slope failure type. Trees growing on a slope that rotationally fails will lean uphill and trees growing on a slope that translationally fails will lean downhill.[Lopez 2010, Schroder, 1978] The way the reaction wood reacts also depends on whether the tree is a Gymnosperm or Angiosperm. Reaction wood of Gymnosperms is accelerated in the direction of the lean and retarded in the direction opposite the lean. Angiosperms react oppositely.[Scurfield 1973]. Landslides that result in large soil disturbances can change the soil water regime of a hillslope. If the soil beneath the tree moves, roots can be damaged, resulting in reduced growth of the entire ring. [Schweingruber, 1996]

For this study, only 6 trees were found suitable for sampling. Location of sampled trees are shown in Figure 11. Tree species included the following: Machilus thunbergii, Pinus taiwanensis, and Alnus formosana makino. Full diameter cores were taken from most trees in the direction parallel and perpendicular to the fall line of the slope.[Lopez, 2010] Samples were collected either at a single height or at two different heights in the bend of the tree.

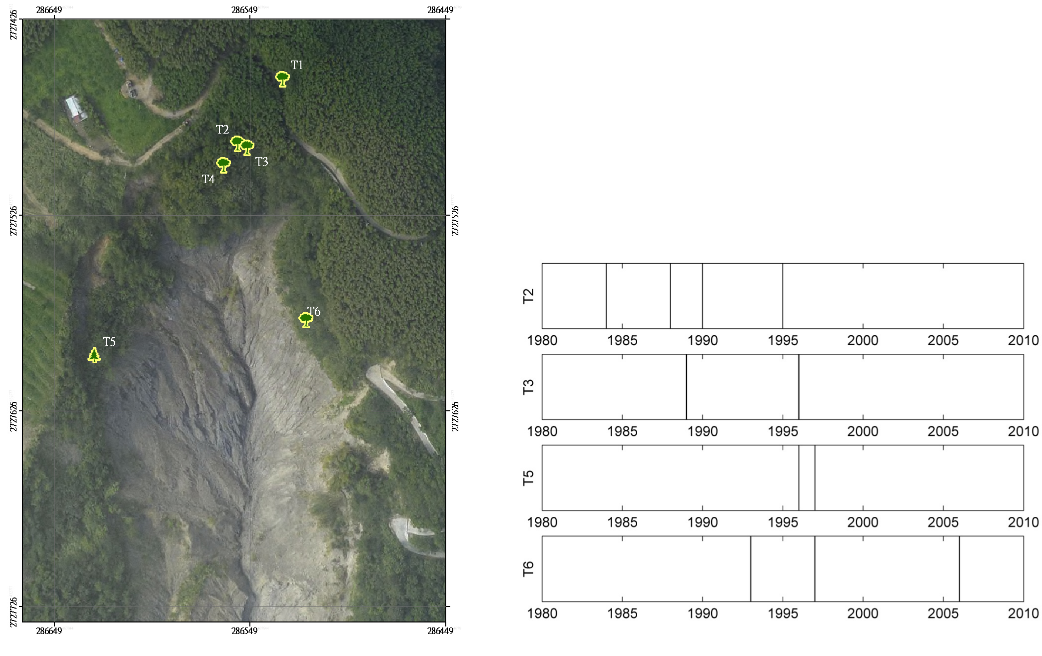


**Fig.11 (left) Locations of trees sampled boarding point source at top of landslide scarp. (right) dates of movement plotted for 4 of the trees: movement shows up in all trees around 1996.**

Once all collected, samples were dried, glued to a supportive piece of wood and sanded three times using successively finer sand paper. 800 grit sand paper was used for the final sanding. Distances between rings were measured using the Quadra-Chek QC10 high precision measuring system. Distances were measured perpendicular to ring growth. Two or more samples from a single tree were simultaneously viewed to ensure correct ring interpretation.

After all measurements were made, data was summarized as cumulative growth and annual growth plots. In some cases the cores intersected rot or did not intersect the tree pith. To help with data interpretation, all data in cumulative plots was translated so that the plotted data intersected at the first year of the shortest core.

Four trees were found to have moved around the year 1996, the year of Typhoon Herb and also first year that the landslide is detected in aerial photo records. According to the tilt direction, the area upslope of the point source rotationally failed and to the sides of the point source, translationally failed. Trees that grew reaction wood around 1996 are plotted on the 1997 aerial photo graph of Tieliku and shaded according to lean type in Figure 12.

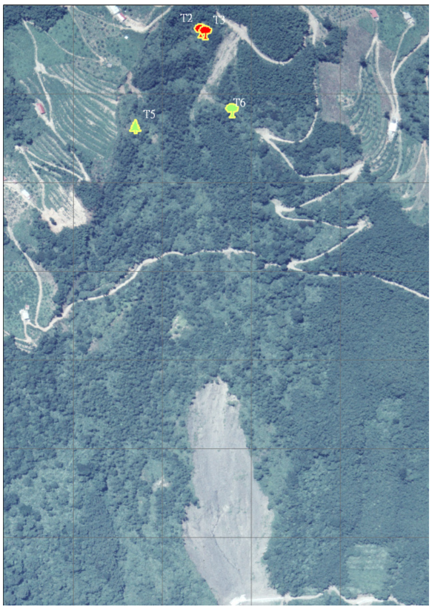

**Fig. 12 Trees that moved in 1997 plotted on the 1997 aerial photo of Tieliku. Light shaded trees signify translational movement. Dark shaded trees signify rotational movement**

## Conclusion

Initial failure, regardless of water input type, resulted in similar landslide scarp geometry. However, further upslope expansion of the scarp depended very much on the water input type. Point source only experiments (PST1 and PST2) were dominated by narrow, upslope scarp growth, which resulted in a decreasing W/SD ratio relative to slope position. Lateral expansion nearly equaled upslope scarp growth for the Rain experiments, which resulted in a relatively constant W/SD ratios with position on the slope. By applying an especially long rain event on the Rain experiments, W/SD ratios actually increased as the scarp rapidly widened but slowly expanded upslope

Regarding accumulated landslide volume, relative to slope position(l/L), all landslides (including Tieliku) share a common feature: initial landslide volume is large relative to subsequent landslide volumes that occur further up the slope. Without an exceptionally long rain event, rain caused slope failures produce little sediments after initial failure. Point source failures however, continue to grow upslope, and in cases that include the effects of bedrock hollows or heavy rain, such as the RainPS experiments, continue to generate large landslide volumes.

Two trends were observed in the surface deformation plots: the existence and non-existence of hillslope deformation above the landslide scarp. All experiments show movement adjacent to the landslide scarp. However, Rain experiments show no evidence of movement upslope of the scarp while the PS experiments do show movement far upslope of the scarp at the location of the point source of bedrock water. These findings could aid in the design of tree ring studies.

A tree ring study performed on trees boarding the edge of the point source at Tieliku revealed that the initial landslide scarp that formed in1997 was paired with deformation on the hillslope far above the scarp. This finding suggests that like the PS experiments, bedrock water played a crucial role in the evolution of the Tieliku landslide and that W/SD and sediment production trends which resemble PS experiment results are not a coincidence.

**References**

Heavy Rain, Extreme Heavy Rain Definition
Taiwan Central Weather Bureau:
http://www.cwb.gov.tw/V7/observe/rainfall/define.htm?

林伯勳博士，冀樹勇博士，鄭錦桐博士,許振崑,梁惠儀,何幸娟,蕭震洋,高丞瑋,尹一帆. (2010) . Study on Historical Migration and Its Mechanism of Heavy Rainfall-Induced Sediment Disaster in Shih-Men Watershed, 財團法人中興工程顧問社(Sinotech Engineering Consultants, Inc.)

徐美玲，廖偉國，(2008) 臺灣的地形，臺灣地理百科，遠足文化,60-61 頁

Dane, J.H. and Topp, G.C Eds. (2002). Methods of Soil Analysis, Part 4, Physical Methods, SSSA Book Series: 5, Madison, Wisconsin, USA, pp.207-208

Eckersley, J.D.(1990). Instrumented laboratory flowslides. Geotechnique 40, No.3, 489-502

Huang Y.F., Huang Y.L Capart,H,(2010) Joint mapping of bed elevation and flow depth in microscale morphodynamics experiments, Experiments in Fluids, Vol. 49, No. 5 pp. 1121.

Hua S.J, (2005). A study of the relationship between landslides and weathering rates of the south cross-island highway, Masters Thesis, National Central University, Taiwan

Iverson, R.M., Reid, M.E., LaHusen, R.G. (1997). Debris-flow mobilization from landslides. Ann. Rev. Earth Planet. Sci. 25,85-138

Iverson, R.M., Reid, M.E., Iverson, N.R., LaHusen, R.G., Logan, M., Mann, J.E., Brien, D.L(2000). Acute Sensitivity of Landslide Rates to Initial Soil Porosity, Science, Vol. 290 pp. 513-516

Jones, Anthony(1971). Soil Piping and Stream Channel Initiation, Water Resources Research, Vol. 7, No. 3, PP. 602-610

Kastning, EH, Faults as Positive and Negative Influences on Ground-Water Flow and Conduit Enlargement; Hydrologic Problems in Karst Regions; Proceedings of Symposium held at Western Kentucky University, Bowling Green, Kentucky April 26-29, 1976.

Keck,J. and Capart, H.(2010) Tieliku landslide, northern Taiwan: Possible role of focused bedrock exfiltration tested using a laboratory analogue, Masters Thesis, National Taiwan University, Taiwan

Kramer, Paul Jackson(1979) Physiology of woody plants. Academic Press, inc.
p. 572-574

Lopez-Saez,J.et al(2010) The Forest: An Efficent Spatio-Temporal Bioindicator of Landslide Activities, a paper presented at International Symposium in Pacific Rim, Taipei, Taiwan

Lin, C.H., Chang, J.C The Discharge and Sediment Load of Heavy Rainfall Events in the Tseng Wen River Basin, Southern Taiwan. (2007) Journal of Geographical Science(48) 43-65

Lopez-Saez J, Corona, C., Gotteland, A., Stoffel., M, Berger, F., Liebault, F.(2010) Dendrogeomorphological reconstruction of past debris-flow events on the Manival torrent(French Alps), a paper presented at International Symposium in Pacific Rim, Taipei, Taiwan

Lourenco, S.D.N., Sassa, K., Fukuoka, H. (2006). Failure process and hydrologic response of a two layer physical model: Implications for rainfall-induced landslides, Geomorphology 73, 115-130

McDonnell, J.J (1990). The influence of macropores on debris flow initiation, Q. J. Engineering Geology, London, 1990, Vol. 23, 325-331.

Montgomery, D.R., Dietrich, W.E., Heffner, J.T. (2002). Piezometric response in shallow bedrock at CB1: Implications for runoff generation and landsliding. Water Resources Research, Vol. 38, No. 12, 1274

Montgomery, D.R., Schmidt, K.M., Dietrich, E.D., McKean, (2009). Instrumental record of debris flow initiation during natural rainfall: Implications for modeling slope stability., Journal of Geophysical Research, Vol. 114

Ni and Capart, (2005). Groundwater drainage and recharge by geomorphically active gullies. MS Thesis, National Taiwan University

E. M. O'Loughlin, (1986). Prediction of Surface Saturation Zones in Natural Catchments by Topographic Analysis. Water Resources Research, Vol. 22, No 5. pp. 794-894

Pierson, T.C.(1977). Factors controlling debris-flow initiation on forested hillslopes in the Oregon Coast Range. Dissertation, PhD Univ. Washington, Seattle

Pierson, T.C. (1983). Soil pipes and slope stability. Q.J. Engineering Geology, London, 1983 Vol. 16, 1-11

Schweingruber, F.H., (1996). Tree Rings and Environment. Dendroecology.

Birmensdorf, Swiss Federal Institute for Forest, Snow and Landscape Research.

Berne, Stuttgart, Vienna, Haupt. pp. 609

Scurfield, G. (1973), Reaction Wood: Its Structure and Function, Science, Vol. 179, pp. 647-655

Shroder, Jr. J.F., (1978), Dendrogeomorphological analysis of mass movement on Table Cliffs Plateau, Utah , Quaternary Research 9, 168-185

Wang, G. and Sassa, K. (2001) Factors affecting rainfall-induced flowslides in laboratory flume tests. Geotechnique 51, No. 7, 587-599

Wang, G., Sassa, K. (2003). Pore-pressure generation and movement of rainfall-induced landslides: effects of grain size and fine particle content. Eng. Geology, 69. 109-125